



UPPSALA  
UNIVERSITET

*Digital Comprehensive Summaries of Uppsala Dissertations  
from the Faculty of Science and Technology 38*

# Classical and Car-Parrinello Molecular Dynamics Simulations of Polyvalent Metal Ions in Water

SAMI AMIRA



ACTA  
UNIVERSITATIS  
UPSALIENSIS  
UPPSALA  
2005

ISSN 1651-6214  
ISBN 91-554-6211-1  
urn:nbn:se:uu:diva-5742

Dissertation presented at Uppsala University to be publicly examined in Polhemsalen, The Ångström Laboratory, Uppsala, Friday, April 29, 2005 at 10:15 for the degree of Doctor of Philosophy. The examination will be conducted in English.

#### **Abstract**

Amira, S. 2005. Classical and Car-Parrinello Molecular Dynamics Simulations of Polyvalent Metal Ions in Water. Acta Universitatis Upsaliensis. *Digital Comprehensive Summaries of Uppsala Dissertations from the Faculty of Science and Technology* 38. vi+39 pp. Uppsala. ISBN 91-554-6211-1.

The aqueous solvation of metal ions is one of the long-standing and complex problems in chemistry, with implications for and applications in a broad range of biochemical and electrochemical systems, where water is the all-pervasive medium.

This thesis describes computer simulations of  $\text{Al}^{3+}(\text{aq})$ ,  $\text{Fe}^{2+}(\text{aq})$ ,  $\text{Fe}^{3+}(\text{aq})$  and  $\text{Cu}^{2+}(\text{aq})$ . Various aspects of the solvation of these polyvalent metal ions in water are addressed, at different levels of theory, using Car-Parrinello molecular dynamics, classical molecular dynamics and quantum-mechanical cluster calculations. Polyvalent metal ions are particularly interesting because of their large influence on the solvent structure, dynamics and thermodynamics, as well as on the properties of the individual solvent molecules. Polyvalent metal ions in aqueous solution also constitute a challenging subject for computer simulations since a sophisticated interaction model is needed to incorporate the large many-body effects.

All the ion-water coordination figures in this thesis are octahedral, except in the  $\text{Cu}^{2+}(\text{aq})$  solution, where the ion is penta-coordinated with four equatorial neighbours in a plane and one axial neighbour located  $\sim 0.45$  Å further out from the ion. The equatorial ion-water bonds have covalent character, while the axial water molecule is only electrostatically bound. For all the ions, the OD stretching frequencies of the first-shell water molecules are much more downshifted than in liquid water. In the case of  $\text{Cu}^{2+}(\text{aq})$ , however, only the OD frequencies of the equatorial water molecules are downshifted with respect to bulk water whereas the OD frequencies of the axial water molecule are slightly upshifted.

Various limitations of the Car-Parrinello molecular dynamics simulations have been explored and compared, such as finite system-size effects and shortcomings in the electronic structure calculations. The Car-Parrinello simulations are found to give reasonable descriptions of the polyvalent metal ions in aqueous solution.

*Keywords:* Car-Parrinello molecular dynamics simulations, ab initio calculations, ion, copper, aluminium, metal ion, water, aqueous solution, solvation

*Sami Amira, Department of Materials Chemistry, Box 538, Uppsala University, SE-75121 Uppsala, Sweden*

© Sami Amira 2005

ISSN 1651-6214

ISBN 91-554-6211-1

urn:nbn:se:uu:diva-5742 (<http://urn.kb.se/resolve?urn=urn:nbn:se:uu:diva-5742>)

## List of Papers

- I. Derivation and evaluation of a flexible SPC model for liquid water**  
S. Amira, D. Spångberg and K. Hermansson  
*Chem. Phys.* **303** (2004) 327
- II. Molecular Dynamics simulation of  $\text{Fe}^{2+}(\text{aq})$  and  $\text{Fe}^{3+}(\text{aq})$**   
S. Amira, D. Spångberg, M. Probst and K. Hermansson  
*J. Phys. Chem. B* **108** (2004) 496
- III. Car-Parrinello Molecular Dynamics simulation of  $\text{Fe}^{3+}(\text{aq})$**   
S. Amira, D. Spångberg, V. Zelin, M. Probst and K. Hermansson  
*J. Phys. Chem. B* (in press).
- IV. Distorted fivefold coordination of  $\text{Cu}^{2+}(\text{aq})$  from a Car-Parrinello Molecular Dynamics Simulation**  
S. Amira, D. Spångberg and K. Hermansson  
Submitted to *Physical Chemistry Chemical Physics*
- V. OD vibrations and hydration structure in an  $\text{Al}^{3+}(\text{aq})$  solution from a Car-Parrinello molecular dynamics simulation**  
S. Amira, D. Spångberg and K. Hermansson  
Submitted to *J. Chem. Phys.*



# Contents

|       |  |    |
|-------|--|----|
| 1     | Introduction   | 3  |
| 2     | Computational methods  | 9  |
| 2.1   | Classical Molecular Dynamics simulations                               | 9  |
| 2.2   | Quantum-mechanical calculations  | 10 |
| 2.2.1 | Hartree-Fock theory and beyond Hartree-Fock                            | 10 |
| 2.2.2 | Density Functional Theory  | 11 |
| 2.3   | Car-Parrinello MD simulations  | 12 |
| 3     | Structural properties  | 15 |
| 3.1   | Structure of the first and second hydration shells                     | 16 |
| 3.2   | The hydration of the cupric ion  | 17 |
| 3.3   | Distance between the first and second hydration shells                 | 20 |
| 3.4   | Angular distribution of the water molecules around the metal ions      | 22 |
| 4     | Intramolecular vibrational properties of the water molecule            | 25 |
| 4.1   | Experimental OH/OD frequencies   | 25 |
| 4.2   | How to compute vibrational frequencies                                 | 25 |
| 4.2.1 | The “classical VAC-FT” spectra   | 26 |
| 4.2.2 | The “quantum-mechanical” anharmonic frozen-field spectra               | 26 |
| 4.2.3 | The harmonic frozen-field spectra                                      | 27 |
| 4.2.4 | Harmonic normal-coordinate analysis from <i>ab initio</i> calculations | 27 |
| 4.3   | Vibrational frequencies: results from the simulations                  | 27 |
| 4.3.1 | Vibrations of the water molecule in the gas-phase                      | 27 |
| 4.3.2 | Vibrations of the water molecule in the pure liquid                    | 27 |
| 4.3.3 | Vibrations of the water molecule in the solution                       | 28 |
| 4.4   | Vibrational frequencies from CPMD simulations versus experiment        | 30 |
| 4.4.1 | The CPMD box-size  | 30 |
| 4.4.2 | The fictitious electron mass parameter in CPMD simulations             | 31 |
| 4.4.3 | The BLYP functional  | 31 |
| 4.4.4 | Anharmonicity effects  | 31 |
| 5     | Summary and concluding remarks   | 33 |
| 6     | Acknowledgments  | 35 |



## Svensk sammanfattning

Joner i lösning är viktiga för många (elektro)kemiska, biologiska och geologiska processer. Järn- och kopparjoner i vatten spelar till exempel en livsviktig roll i ett stort antal biokemiska reaktioner i vår kropp. Halten av aluminium i levande organismer däremot är mycket ringa och tycks ha en skadlig inverkan i kroppen.

Centrala temat för denna avhandling är teoretiska beräkningar av struktur och dynamik av vattenmolekyler kring metalljoner. Teoretiska beräkningar ger oss grundläggande förståelse och detaljerad information på atomär och molekylär nivå, som ibland kan vara svårt att erhålla med experiment. Klassiska molekylär dynamik(MD)-simuleringar har använts för att studera joner i lösning i drygt 30 år. Växelverkan mellan vattenmolekyler och joner beskrivs här av ett så kallat kraftfält (dvs förenklade analytiska uttryck för atomernas växelverkan). Fördelen med sådana simuleringar är att de inte tar så orimligt mycket beräkningstid. Nackdelen är att elektroniska effekter inte finns med direkt i beskrivningen. Från kvantmekaniska ("ab initio") beräkningar, å andra sidan, kan man räkna fram statistiska egenskaper, dvs vid 0 Kelvin. Att kombinera MD-simuleringar och kvantmekanik till "ab initio" molekylärdynamik, har de senaste åren blivit ett intressant alternativ tack vare den fortsatta utvecklingen av datorkraft och algoritmer. Car-Parrinello molekylärdynamik (CPMD), den mest kända variant av "ab initio" molekylärdynamik, har använts i denna avhandling som huvudsakliga metod.

Men CPMD är en ganska ny metod och därför är det viktigt att kartlägga vilka egenskaper som blir bättre och vilka egenskaper som blir sämre jämfört med klassiska MD simuleringar. Med CPMD kan man till exempel bara ha små system. Mina simuleringar av en trivalent järnjon i vatten ger ett bra exempel av de möjligheterna CPMD erbjuder och de begränsningar som finns. Jag har gjort så liknande som möjligt klassiska och CPMD simuleringar för att undersöka detta.

I vattenlösning formerar sig vattenmolekyler runt jonerna i ett akvacomplex vilket gör att jonerna uppträder som större strukturer än enbart jonen. Med CPMD metoden omges järn- och aluminiumjoner närmast av 6 vattenmolekyler i lösning medan däremot koppar bara omges av fem molekyler.

CPMD metoden är särskild bra för simulering av lösningar där elektrostruktur spelar en stor roll, eftersom sådana effekter inte beskrivs på ett

tillräckligt bra sätt av klassisk MD. Solvatering av kopparjoner i vatten är ett sådant fall.

Tyngdpunkten för forskningsarbetet ligger på strukturella och dynamiska egenskaper. Förutom de egenskaper man får från klassiska MD, kan man med CPMD simuleringar även räkna fram helt nya egenskaper, nämligen egenskaper knytan till den elektroniska strukturen i lösning. Djupare insikt i den elektroniska strukturen i lösning kan i framtiden bidra till en ökad förståelse av till exempel elektrokemin och kasta ett nytt ljus på lösningskemi.

# Introduction

The main subject of this thesis is in the field of coordination chemistry, namely a theoretical investigation of the solvation of polyvalent metal ions in water. Water is one of the most fascinating substances present on this planet with truly unique properties. The explanation for the unusual behaviour of water is found in the so-called hydrogen bonding, and water is in this regard indeed special since it can act both as a hydrogen bond donor and acceptor. Hydrogen bonds are for instance also responsible for the double helix shape in DNA and the perfect mixing of ethanol and water. One of the most important properties of water is its ability to dissolve ions and polar molecules to form liquid solutions.

In nature, water contains a vast number of dissolved substances, which are vital to life. Moreover, in living organisms, water enables the transport of nutrients and trace elements. Solvation involves complex rearrangements of the solvent and the solute, where the polar nature of the water molecule and the hydrogen bond making and breaking play a crucial part [1]. The structure and dynamics of the solvent are intimately connected to the way in which chemical reactions in water take place. Acid-catalyzed reactions in aqueous solution, for instance, in which protons rapidly move along the hydrogen-bond network through the solvent by passing on hydrogens from water molecule to water molecule, are well known examples. The dynamic solvent effects and the key role of water in chemical reactions are still not very well understood at a microscopic level.

The experimental determination of the solvent structure and dynamics is not trivial and the results are often subject to large uncertainties. Molecular simulations are very useful in providing the detailed molecular-level information about the solvation, giving access to properties that experimentally are very difficult to obtain and being helpful in the interpretation of experimental data.

To obtain reliable molecular-level information, high-quality simulations are needed. The focus in this thesis work is on molecular dynamics (MD) simulations. Several factors affect the quality of the simulations: the system size, the length of the simulation, and crucially the potential model. The most simple way to construct the potential model is by adding together the interactions between all the pairs of atomic interaction sites in the system. However, the interaction between two molecules is affected by the presence of a third, fourth or more molecules, resulting in non-pairwise contributions, so-called *many-*

*body effects.* Many-body effects are particularly strong when polyvalent metal cations are present in aqueous solution because the cations strengthen cooperative hydrogen-bonding in the water network around them due to the polarization of water O-H by cation-lone pair interactions (Cation<sup>n+</sup>...O-H<sub>2</sub>...O-H<sub>2</sub>).

The interaction models can be classified according to the way the many-body effects are taken into account. The analytical potential expression for an N-body system  $V = V(\vec{r}_1, \dots, \vec{r}_N)$ , can be written as an expansion of the coordinates  $(\vec{r}_1, \dots, \vec{r}_N)$  in the following way:

$$V = \sum_{i=1}^N \sum_{j>i}^N v_2(\vec{r}_i, \vec{r}_j) + \sum_{i=1}^N \sum_{j>i}^N \sum_{k>j}^N v_3(\vec{r}_i, \vec{r}_j, \vec{r}_k) + \dots \quad (1.1)$$

where the N-body term is the last one in the expansion. The simplest interaction models, the pure 2-body potentials, take only the sum of the pairwise interactions (the first term in equation 1.1) into account. It is possible to include a significant part of the many-body effects in pairwise potentials in an average way with “effective” pair potentials. In such a case the potential energy does not represent the true interaction energy of the two particles. The inclusion of more terms in the potential expression leads to pure or effective 3-body potentials, and so on. The computational cost increases significantly if higher-order terms are included. Nowadays simulations on the nanosecond timescale are affordable for 3-body potentials.

Another way to handle the many-body effects is to use a potential model that explicitly includes polarisation [2]. Different ways to include polarisation are the use of isotropic or anisotropic molecular polarisabilities, atom-centred polarisabilities or the variable charge method. The cost of using polarisable potentials is usually higher than that of the simpler 2- or 3-body potentials.

QM/MM-MD is a quite recent method, where the immediate surrounding of the ion is treated by an *ab initio* calculation at every timestep and the remaining part by empirical effective potentials (see Refs. 3–6 for a number of recent examples). This means that inside the QM region *all* many-body effects are included. Given the high computational cost of *ab initio* calculations, however, the QM-region is currently limited to the water molecules that are in the first two hydration shells of the ion. The high computational cost also limits the simulation time to a few tens of picoseconds, a couple of orders of magnitude smaller than for polarizable models.

Car-Parrinello molecular dynamics (CPMD) simulations do not rely on analytical force fields but rather determine the potential energy surface from first principles on the fly [7]. The interactions between the atoms are in other words calculated from first principles at every time-step. The nuclei are treated as classical particles and the electrons with density functional theory (DFT) [8]. Here, all the many-body effects are in principle included in the simulation. Currently, the expense of CPMD simulations usually limits the system-size to

less than 100 water molecules and the simulation time to a few ten picoseconds.

In the description above the interaction models become more “sophisticated” or “formally” more advanced if we go from MD simulations using pair-potentials to three-body to polarisable to QM/MM-MD to CPMD. However, examples show that in specific cases and for certain properties, a pair potential can do equally well or outperform a CPMD simulation, when compared with certain experimental results. The empirical potential for  $\text{Fe}^{3+}$  versus the CPMD simulation in Paper IV is such an example, where the experimental frequency is better reproduced by the more simple model. Some of the reasons for this may be that a classical MD simulation can afford longer simulation times and larger system sizes, and that, in fact, the pair potential may have been parameterised in a very appropriate way for the system under study, while the errors and approximations inherent in the density functional method and the pseudo-potential chosen in the CPMD approach may be larger.

To date, approximately a dozen CPMD publications have appeared in the literature for metal cations in aqueous solution and they are listed in Table 1.1. They were all performed for  $\sim 300$  K and the fictitious electron mass used was in the range 680 to 1100 a.u.

*Table 1.1:* A summary of the CPMD simulations of metal cations in aqueous solution which have appeared in the literature. The “PP” column lists the pseudo-potentials (Vanderbilt, Troullier-Martins or Projector Augmented Waves) used,  $E_{\text{cut}}$  refers to the plane-wave cutoff value and the next column uses abbreviations to list the main quantities studied such as the radial distribution function, intramolecular vibrations, Wannier functions, tilt angle, chemical and redox reactions and XANES spectra.

| System   | Ensemble       | Functional | PP  | $t_{\text{run}}$ (ps) | $E_{\text{cut}}$ (Ryd) | Main quantities studied            | Reference |
|--|----------------|------------|-----|-----------------------|------------------------|------------------------------------|-----------|
| 1 $\text{Li}^+$ + 32 $\text{H}_2\text{O}$      | NVT            | BLYP       | VdB | 20.0                  | 25                     | Rdf, tilt, $\omega(\text{OH})$     | [9]       |
| 1 $\text{Be}^{2+}$ + 31 $\text{D}_2\text{O}$   | NVE            | B          | VdB | 1.0                   | 24                     | Rdf, tilt                          | [10]      |
| 1 $\text{Na}^+$ + 53 $\text{D}_2\text{O}$      | NVE            | PBE        | TM  | 2.85                  | 85                     | Rdf, tilt                          | [11]      |
| 1 $\text{Na}^+$ + 33 $\text{H}_2\text{O}$      | NVT            | BLYP       | TM  | 5.0                   | 70                     | WF                                 | [12]      |
| 1 $\text{Mg}^{2+}$ + 53 $\text{D}_2\text{O}$   | NVE            | PBE        | TM  | 3.1                   | 85                     | Rdf, WF                            | [13]      |
| 1 $\text{Al}^{3+}$ + 62 $\text{D}_2\text{O}$   | NVE            | HCTH       | TM  | 28.0                  | 70                     | Rdf, tilt, WF                      | [14]      |
| 1 $\text{Al}^{3+}$ + 32 $\text{D}_2\text{O}$   | NVT            | BLYP       | VdB | 10.0                  | 60                     | Rdf, tilt, $\omega(\text{OD})$     | Paper V   |
| 1 $\text{K}^+$ + 59 $\text{D}_2\text{O}$       | NVE            | BLYP       | TM  | 1.98                  | 70                     | Rdf, tilt                          | [15]      |
| 1 $\text{Ca}^{2+}$ + 54 $\text{D}_2\text{O}$   | NVE            | BLYP       | TM  | 7.0                   | 70                     | Rdf, WF                            | [16]      |
| 1 $\text{Ca}^{2+}$ + 31 $\text{D}_2\text{O}$   | NVE            | BLYP       | TM  | 14.2                  | 80                     | Rdf, tilt                          | [17]      |
| 1 $\text{Fe}^{2+}$ + 31 $\text{D}_2\text{O}$   | NVT            | BP         | PAW | short runs            | 30                     | Rdf, CR                            | [18]      |
| 1 $\text{Fe}^{3+}$ + 32 $\text{D}_2\text{O}$   | NVT            | BLYP       | VdB | 7.0                   | 60                     | Rdf, tilt, $\omega(\text{OD})$     | Paper III |
| 1 $\text{Cu}^{2+}$ + 50 $\text{D}_2\text{O}$   | NVE            | BLYP       | VdB | 17.0                  |                        | Rdf, XANES                         | [19]      |
| 1 $\text{Cu}^{+/2+}$ + 32 $\text{H}_2\text{O}$ | $\mu\text{VT}$ | BLYP       | TM  | 2-3                   | 70                     | Rdf, redox                         | [20]      |
| 1 $\text{Cu}^{2+}$ + 32 $\text{D}_2\text{O}$   | NVT            | BLYP       | VdB | 18                    | 60                     | Rdf, tilt, WF, $\omega(\text{OD})$ | Paper IV  |
| 1 $\text{Ag}^+$ + 32 $\text{H}_2\text{O}$      | NVT            | BLYP       | TM  | 5.0                   | 70                     | WF                                 | [12]      |
| 1 $\text{Ag}^{+/2+}$ + 32 $\text{H}_2\text{O}$ | $\mu\text{VT}$ | BLYP       | TM  | 2-3                   | 70                     | Rdf, redox                         | [20]      |

The overall aims of this thesis are (at least) two-fold. (1) To study the first and second hydration-shell structure and dynamics of some polyvalent metal ions (transition metal and non-transition metal) in aqueous solution. (2) To evaluate the performance, advantages and limitations of the CPMD method for the study of metal ions in aqueous solution. More specifically the following questions are addressed in this thesis summary and in the separate papers:

- Do CPMD simulations return a hydration structure that agrees with the available experimental data?
- The CPMD simulation technique naturally includes all the many-body effects in the solution. For which properties can we see the clearest impact?
- How much does the small system-sizes affect the calculated properties of the solutions?
- Comparing a CPMD simulation with an as similar as possible classical MD simulation, for which properties will the differences be most clear?
- CPMD simulations give access to the electronic structure at every timestep. Can the electronic structure of the solution contribute to a better understanding of the ionic solvation?
- Do the polyvalent ions affect the water molecules more than the bulk?
- The description of the electron density using pseudo-potentials and plane-waves in combination with a certain exchange-correlation functional is an important approximations in CPMD. How important is the error that we introduce by this approximation? And how can the description of the electron density be improved?
- Can we construct a flexible water model that generates reliable O-H frequencies and frequency shifts for hydration water?
- Can CPMD simulations generate equally reliable O-H frequencies and frequency shifts for hydration water?

Different types of theoretical calculations for two divalent ( $\text{Fe}^{2+}$  and  $\text{Cu}^{2+}$ ) and two trivalent ( $\text{Al}^{3+}$  and  $\text{Fe}^{3+}$ ) ions, all hydrated, have been studied in this thesis to help answer the questions posed above. The systems are listed in Table 1.2. The  $\text{Al}^{3+}$  ion has the [Ne] noble gas electronic configuration with a closed valence shell, while the *d*-electron metal ions  $\text{Fe}^{2+}$  ( $[\text{Ar}]3d^6$ ),  $\text{Fe}^{3+}$  ( $[\text{Ar}]3d^5$ ) and  $\text{Cu}^{2+}$  ( $[\text{Ar}]3d^9$ ) have unfilled valence shells. Transition metal ions have, because of the presence of *d*-electrons in their electronic structures, a very rich chemistry and can be involved in complex bonding situations with

*Table 1.2:* Schematic overview of the calculations and simulations in this dissertation. CPMD and CLMD refer to Car-Parrinello and classical MD simulations. The QC column refers to static quantum-mechanical cluster calculations with geometry optimization.

|   | QC      | CPMD    | CLMD    | Reference              |
|---|---------|---------|---------|------------------------|
| H <sub>2</sub> O( <i>g</i> )  | 1       | 1       | 1       | Papers <b>I,II</b>     |
| H <sub>2</sub> O( <i>l</i> )  | –       | –       | 512     | Papers <b>I,II</b>     |
| D <sub>2</sub> O( <i>g</i> )  | 1       | 1       | 1       | Papers <b>III,IV,V</b> |
| D <sub>2</sub> O( <i>l</i> )  | –       | 32      | 32      | Papers <b>III,IV,V</b> |
| Fe <sup>2+</sup> ( <i>aq</i> )                                      | –       | –       | 512     | Paper <b>II</b>        |
| Fe(D <sub>2</sub> O) <sub><i>n</i></sub> <sup>3+</sup> ( <i>g</i> ) | 4,6     | 4,6     | –       | Paper <b>III</b>       |
| Fe <sup>3+</sup> ( <i>aq</i> )                                      | –       | 32      | 32, 512 | Papers <b>II,III</b>   |
| Cu <sup>2+</sup> ( <i>aq</i> )                                      | –       | 32      | –       | Paper <b>IV</b>        |
| Al(H <sub>2</sub> O) <sub><i>n</i></sub> <sup>3+</sup> ( <i>g</i> ) | 1,2,4,6 | 1,2,4,6 | –       | Paper <b>V</b>         |
| Al <sup>3+</sup> ( <i>aq</i> )                                      | –       | 32      | –       | Paper <b>V</b>         |

ligands. A qualitative estimate of the bonding character is often attained by using the empirically derived concept of electronegativity (see Table 1.3 for electronegativity values for the metal ions and the solvent in this work). From the tabulated values it appears that the metal ions studied here are, despite the fact that they have pairwise the same oxidation number, chemically very different. This idea was rationalised and generalised in the late 1960s by Pearson in the well known HSAB principle [21, 22], stating that hard acids prefer to coordinate to hard bases and soft acids to soft bases. The connection to the intermolecular interactions is that soft acids and bases are largely covalently bound and hard acids and bases are mainly ionically bound. This is quantified on the scale of absolute hardness,  $\eta$ ; values for the absolute hardness for the metal ions and the solvent are shown in Table 1.3. On this scale the Al<sup>3+</sup> ion is a hard acid and the Fe<sup>2+</sup>, Fe<sup>3+</sup> and Cu<sup>2+</sup> ions are acids of intermediate strength coordinating to H<sub>2</sub>O, a hard base. We can expect the electrostatics to be dominating, with the covalent character increasing from Fe<sup>3+</sup> over Cu<sup>2+</sup> to Fe<sup>2+</sup>. HSAB does not explain variations in the strength of the chemical bonding. The charge/radius ratio can be used to evaluate the strength of the chemical bonding. Values for the Shannon’s effective ionic radii for the metal ions in this work [23] and a value for the radius of the solvent molecule [24] are given in Table 1.3. Judging from the charge/radius ratio we can expect Al<sup>3+</sup> to bind considerably stronger than the transition metal ions.

*Table 1.3:* Pearson's values of absolute hardness,  $\eta$ , and absolute electronegativity,  $\chi$  ( in eV) and Shannon's effective ionic radii (in Å for the metal ions and the solvent.  $\eta$  is defined as  $\eta = (I - A)/2$  where I is the ionisation potential and A is the electron affinity.  $\chi$  is defined as  $\chi = (I + A)/2$ , based on the Mulliken scale.

|        | Fe <sup>2+</sup> | Cu <sup>2+</sup> | Al <sup>3+</sup> | Fe <sup>3+</sup> | H <sub>2</sub> O |
|--------|------------------|------------------|------------------|------------------|------------------|
| $\eta$ | 7.24             | 8.27             | 45.77            | 12.08            | 9.5              |
| $\chi$ | 23.42            | 28.56            | 74.22            | 42.73            | 3.1              |
| r      | 0.78             | 0.65             | 0.39             | 0.645            | 1.34             |

The thesis outline is as follows. Chapter 2 gives a brief description of the computational methods that have been used in this thesis. In chapters 3 and 4, a summary of the simulation results for the structural and vibrational properties of the ionic solutions is presented. The last chapter contains a summary of this work and concluding remarks.

# Computational methods

The aim of the present chapter is to present a short, non-technical description of the computational chemistry methods that are used in this thesis. A more in depth and complete coverage of the computational methods is found in the relevant textbooks or review articles. Below three computational chemistry methods are described. The classical molecular dynamics approach gives a dynamical picture and allows for the calculation of large systems but uses a rather simple model to describe the molecular interactions. The quantum-mechanical *ab initio* approaches give a static picture and use a more precise model to describe the molecular interactions, but only systems with a small number of molecules can be studied. The Car-Parrinello MD approach combines in an elegant theoretical framework molecular dynamics with quantum-mechanics.

## 2.1 Classical Molecular Dynamics simulations

Classical molecular dynamics simulations rely on the theory of statistical mechanics and are based on the integration of Newton's equations of motions for interacting particles. Newton's equations of motion are solved for all particles simultaneously: using a finite difference method the particles are moved forward by integrating over time in small increments. A typical timestep is  $10^{-15}$ s. The velocity Verlet integrator [25] was used to integrate the equations of motion for all MD simulations in this thesis work.

The interactions are described by a rather simple model of the interactions in the system, i.e. by analytical potentials, which can be further divided in two classes: empirical potentials and *ab initio* potentials. Empirical  $\text{Fe}^{n+}$ -water potentials by Curtiss et al. [26] and empirical water-water potentials have been used in this dissertation for the simulation of  $\text{Fe}^{2+}(aq)$  and  $\text{Fe}^{3+}(aq)$  in Papers **II** and **III** as well as for the simulation of pure liquid water in Paper **I**. The empirical potentials are built up by fitting the parameters in the potential expression to a set of experimental data. The parameters in the *ab initio* potentials on the other hand are built up from quantum-mechanical calculations. The simulation generates representative configurations in phase-space in such a way that average values of structural and thermodynamical properties can be obtained. Molecular dynamics also allows for the computation of the time-dependent properties of atomic or molecular systems and allows one to

monitor the the changes from one configuration to another. Periodic boundary conditions enable the calculation of macroscopic properties from simulations with a relatively small number of particles and are therefore a crucial feature of the simulation set-up. Here, the simulations have been carried out in the NVT (constant number of particles, volume and temperature) ensemble, where the temperature was kept constant using the extended-system method of Nosé and Hoover [27,28]. The long-ranged Coulombic interactions were handled by the Ewald summation technique [29] .

## 2.2 Quantum-mechanical calculations

The solution of the time independent Schrödinger equation returns, the wave function  $\psi$  (and eigenvalues) that determines all the physical properties of the system, is the key to the description of the electronic structure of atoms and molecules. Unfortunately an exact solution of the Schrödinger equation is impossible to obtain for chemically relevant problems, therefore techniques have been developed to generate approximate solutions. A major simplification is the Born-Oppenheimer approximation, which separates the motion of the electrons from the motion of the nuclei. The price to pay for the access to the electronic structure is the loss of (thermal) motion: the result is a static description of atoms and molecules at 0 Kelvin. The two most popular schemes for solving the Schrödinger equation for atoms and molecules (with approximations) are the Hartree-Fock and Density Functional theory.

### 2.2.1 Hartree-Fock theory and beyond Hartree-Fock

Hartree-Fock theory (see for example Ref. [30], for an introduction) allows one to find approximate solutions for the time independent Schrödinger equation. The wave function in Hartree-Fock theory is approximated by the Slater determinant, an antisymmetrized product of  $N$  orthonormal spin orbitals, with  $N$  being the number of electrons. The spin orbitals are expressed as a linear combination of atomic orbitals (LCAO). The self-consistent field (SCF) approach is used to find solutions for the wave function and the energies. The major disadvantage of the Hartree-Fock theory is that it fails to describe electron correlation, because in the SCF method each electron moves in the "mean-field" of the other electrons. The motions of the electrons are in reality correlated and this results in a lower energy than the Hartree-Fock theory predicts. The correlation energy is thus defined as the difference between the Hartree-Fock energy and the exact energy.

Different methods to take correlation effects into account are for instance Moller-Plesset perturbation theory (MP2, MP3, ...), configuration interaction

(CI) and coupled cluster (CC). In Moller-Plesset perturbation theory the difference between the exact Hamiltonian and the sum of one-electron operators is introduced as a perturbation to the unperturbed Hartree-Fock solution. Correlation corrections can be derived to a chosen order. Another way to take correlation into account is to work with a multi-determinant wave function instead of the single-determinant wave function (Slater determinant). This approach is used in the configuration interaction and coupled cluster methods. The coupled cluster and MP2 methods have been used in the *ab initio* calculations of small  $\text{Al}(\text{D}_2\text{O})_n^{3+}$  clusters in Paper V.

### 2.2.2 Density Functional Theory

The starting point in DFT (see for example Ref. 8 for an introduction) is not the wave function but the electron density. DFT is based on Hohenberg and Kohn's theorem stating that for a many-electron system there is a one-to-one mapping between the external potential and the electron density. This means that the density is uniquely determined given the external potential, and vice versa. Consequently all properties are a functional of the density, because the density determines the external potential, which determines the Hamiltonian, which in turn determines the energy. The total energy of an electron gas, including the many-body effects of the electrons, in the presence of a static external potential (of the nuclei), is then a unique functional of the electron density. The minimum of the total energy functional is the ground state energy of the N-electron system with the nuclei at fixed positions. It was then shown by Kohn and Sham that it is possible to replace the many-electron problem by an exactly equivalent set of self-consistent one electron equations, later known as Kohn-Sham equations. The Kohn-Sham equations represent a mapping of the interacting many-electron system onto a system of non-interacting electrons moving in an effective potential due to all the other electrons. The ground-state energy can be written as:

$$E[\rho] = T[\rho] + E_{ne}[\rho] + J[\rho] + E_{xc}[\rho] \quad (2.1)$$

where  $T[\rho]$  is the kinetic energy,  $E_{ne}[\rho]$  the electron-nucleus interaction,  $J[\rho]$  the classical Coulombic interaction and  $E_{xc}[\rho]$  the exchange-correlation energy. The main problem is that an exact expression for  $E_{xc}[\rho]$  is not known and approximate functionals must be used. The simplest description of the exchange-correlation energy of an electronic system is with functionals that are dependent on the electron density only using the Local Density Approximation (LDA). Generalized Gradient Approximation (GGA) functionals are not only dependent on the electron density but also on the gradient of the electron density and can be considered as an improvement of the LDA. The BLYP and the PBE functionals that have been used in this dissertation are

GGA functionals. DFT can be implemented either with an atom-centred localized basis set or with a plane-wave basis set. We have compared the results of DFT calculations of small  $\text{Al}(\text{D}_2\text{O})_n^{3+}$  clusters in Paper V using both a local basis-set and a plane-wave basis-set.

### 2.3 Car-Parrinello MD simulations

The Car-Parrinello MD method (for a general introduction, see Ref. 31) connects a classical MD treatment of the nuclei with a DFT treatment of the electrons, using an extended-Lagrangian formulation. The characteristic feature of Car-Parrinello MD is that wave function is dynamically optimised to be consistent with the changing positions of the atomic nuclei. This is achieved by giving the electrons a fictitious mass associated with the dynamics of the electronic degrees of freedom. The computational implementation involves the numerical integration of the equations of motion of second-order Newtonian dynamics using finite difference methods just as in classical MD. The fictitious mass has to be chosen in such a way that the wave function adapts quickly to the changing nuclear positions and energy transfer between the electronic and nuclear degrees of freedom is avoided. The essential idea is that once the electrons are put in the ground state (on the Born-Oppenheimer surface) for a certain set of ionic positions, the electronic wave function will follow the motion of the ions adiabatically, performing only small oscillations around the ground state. In this way, parameter-free MD simulations can be performed, in which all interactions are calculated on-the-fly within the DFT framework, instead of from fixed force-fields, as in classical MD.

The electronic wave function is expanded in a plane-wave basis set. The computational cost of an all-electron calculation is very high, because of the large number of plane-waves that are needed to describe the fast fluctuation of the wave function corresponding to the core electrons. This is avoided in the pseudo-potential approximation, where the core electrons and the strong ionic potential of the are replaced by a weaker pseudo-potential. This set-up allows one to truncate the plane-wave with kinetic energies beyond a much smaller cutoff value. The CPMD simulations in this dissertation have been run with Vanderbilt ultra-soft pseudo-potentials [32].

The Car-Parrinello method integrates the fictitious wave function dynamics with the classical MD using a single extended Lagrangian ( $L$ ), that can be written as follows:

$$L_{CP} = \sum_i \mu \langle \dot{\psi}_i | \dot{\psi}_i \rangle + \frac{1}{2} \sum_I M_I \dot{R}_I^2 - E[\{\psi_i\}, R_I] \quad (2.2)$$

where  $\mu$  is the fictitious electron mass,  $\psi_i$  the electronic wave function  $i$ ,  $E$  is the Kohn-Sham energy functional and  $R_I$  is the position of the ion. This

expression corresponds to the conventional form of the Lagrangian where the kinetic energy includes the fictitious dynamics of the electronic wave function and the Kohn-Sham energy functional represents the potential energy of the system. The electronic and ionic degrees of freedom are coupled through the Car-Parrinello Lagrangian and in principle energy can flow from the ionic to the electronic subsystem, leading to deviations from the Born-Oppenheimer surface. A good choice of  $\mu$  will make sure that the frequency spectra of the electronic orbitals and the ions are well separated (energetically isolated) from one another. Using heavier isotopes is an additional way to ensure this separation since it shifts the spectrum for the fastest ionic motion to lower frequencies. This is why the hydrogen atoms have been replaced by deuterium atoms in all the CPMD simulations in this dissertation.

A major advantage of the CPMD methods is that the many-body effects that are very important for polyvalent metal ions, are naturally included. Because the forces on the nuclei are obtained from quantum-mechanical calculations, the electronic structure is available during the molecular dynamics, which can contribute to a better understanding of the chemistry.

Important approximations in CPMD come in the first place from the calculation of the molecular interactions, where DFT sets the limitations. Particularly, current electron exchange-correlation functionals can still be improved and several cases are known where DFT fails. Secondly, the computational demands of CPMD are very high, limiting the system-size to 100-1000 atoms and the length of the simulation to 10-100 picoseconds. This is just enough to include the first and second hydration shells around a metal ion. Several aspects of the dynamics of the solvent, however, take place at timescales that largely exceed 10-100 ps. Exchange around polyvalent transition metal ions, for instance, takes place on a much longer timescale [33] and is currently beyond the reach of CPMD (and of classical MD as well). Techniques to accelerate so-called rare events in CPMD do exist and open the way to simulate complex chemical reactions in condensed phase (see for instance Ref. 34). Other approximations are the neglect of quantum mechanical nuclear effects in the classical dynamics, such as tunneling and zero-point motions (although they can be taken into account approximately, using path-integral methods, at a large computational cost), the use of pseudo-potentials for the core electrons and the Born Oppenheimer approximation. This work addresses some of these issues by testing and critically comparing the DFT model to other methods and to experimental and theoretical results in the literature.



## Structural properties

In this chapter the most important results concerning the local ion hydration structure of the ionic solutions studied in this thesis work are discussed in terms of the distances between the ion and the first and the second-shells, the average coordination numbers and the tilt angle of the water molecules in the hydration shells. The results for the solvation of the cupric ion are presented in a separate section. Figure 3.1 shows an example of the local hydration structure of the ferric ion, as obtained from the trajectory of the CPMD simulation in Paper **III**.

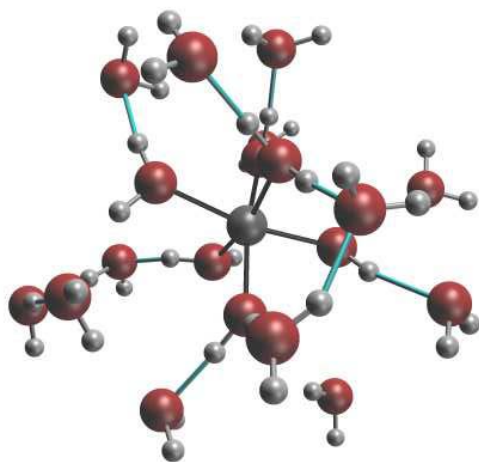


*Figure 3.1:* Snapshot of the water structure around an  $\text{Fe}^{3+}(aq)$  ion obtained from the CPMD trajectory. The water molecules surrounding the ion form an octahedron.

### 3.1 Structure of the first and second hydration shells

Polyvalent metal ions have a strong ordering effect on the surrounding water molecules and this results for instance in short ion-oxygen distances. The distances between the ion and the first and the second-shells and the average coordination number for the different CPMD and classical MD (CLMD) simulations, computed from the ion-oxygen radial distribution functions (RDFs), are collected in Table 3.1 and Table 3.2, respectively.

*Table 3.1:* First hydration shell distances and average coordination numbers, calculated from the different radial distribution functions from the CPMD and the CLMD simulations. The superscript 1 means first hydration shell. Experimental literature values are taken from diffraction experiments (see Ref. 35). All distances are in Å.

| Method/ion | $R(\text{Fe}^{2+}\text{-O}_1)$ | $R(\text{Fe}^{3+}\text{-O}_1)$ | $R(\text{Cu}^{2+}\text{-O}_1)$ | $R(\text{Al}^{3+}\text{-O}_1)$ |
|------------|--------------------------------|--------------------------------|--------------------------------|--------------------------------|
| CPMD-32    | –                              | 2.05(6)                        | 2.00(eq.)/2.45(ax.)            | 1.92(6)                        |
| CLMD-32    | –                              | 1.98(6)                        | –                              | –                              |
| CLMD-512   | 2.09(6)                        | 1.96(6)                        | –                              | –                              |
| Experiment | 2.09-2.28(6)                   | 1.98-2.05(6)                   | [see section 3.2]              | 1.87-1.90(6)                   |

The bond distances for all the ions are in good agreement with those obtained from experiment; the distances from the CPMD simulations are generally in the upper limit of the experimental range of values or just above those values. The bond length increases as  $\text{Al}^{3+} < \text{Fe}^{3+} < \text{Cu}^{2+} < \text{Fe}^{2+}$ , as expected from Shannon’s effective radii (see Table 1.3).

The first hydration shells of  $\text{Al}^{3+}$ ,  $\text{Fe}^{3+}$  and  $\text{Fe}^{2+}$  contain 6 water molecules in octahedral arrangements, in agreement with the experimental results.

*Table 3.2:* Second hydration shell distances and average coordination numbers, calculated from the different radial distribution functions from the CPMD and the CLMD simulations. Experimental literature values are taken from diffraction (see Ref. 35) and IR spectroscopy (see Ref. 36–38). Coordination numbers are given in parenthesis. All distances are in Å.

| Method/ion | $R(\text{Fe}^{2+}\text{-O}_2)$ | $R(\text{Fe}^{3+}\text{-O}_2)$ | $R(\text{Cu}^{2+}\text{-O}_2)$ | $R(\text{Al}^{3+}\text{-O}_2)$ |
|------------|--------------------------------|--------------------------------|--------------------------------|--------------------------------|
| CPMD-32    | –                              | 4.26 (11.5)                    | 4.03 (8)                       | 4.21 (11.2)                    |
| CLMD-32    | –                              | 4.14 (11.0)                    | –                              | –                              |
| CLMD-512   | 4.31 (12)                      | 4.14 (12.5)                    | –                              | –                              |
| Experiment | 4.30-4.51 (12)                 | 4.09-4.80 (5-12)               | 3.95-4.20 (8)                  | 3.99-4.15 (12-14)              |

The ion-second shell distances from the simulations agree with the distances obtained from X-ray diffraction experiments. The significantly longer ion-second hydration shell distance for  $\text{Fe}^{3+}$  in the case of the CPMD simulation (4.26 Å versus 4.14 Å) is not only a result of the longer ion first-shell distance. It is probably connected to a better description of the polarization effects in the CPMD simulation; a similar lengthening has also been observed in classical MD studies with polarizable models (see for instance Ref. 39).

The average coordination number in the second hydration shell appears to be systematically a little too low for the CPMD simulations (see Table 3.2). The comparison of the classical  $\text{Fe}^{3+}(aq)$  simulation with 32 and 512 water molecules in Paper III suggests that this is (at least partly) due to the small system size.

The main results of this section are the following:

- For the first and second hydration shells the resulting CPMD hydration structures are in very good agreement with experimental data whenever such exist.
- The second-shell coordination number is slightly lower for the simulations with 32 water molecules compared to the simulations with 512 water molecules.

### 3.2 The hydration of the cupric ion

The preferred number of coordinating ligands and the coordination geometry of the cupric ion have been at the centre of controversy for quite some time. The  $\text{Cu}^{2+}(aq)$  complex is generally assumed to be a Jahn-Teller distorted octahedron, with four equidistant equatorial water molecules and two axial water molecules at a larger distance. Structural studies on the cupric ion complex using different experimental methods have come to diverging conclusions concerning the coordination around the  $\text{Cu}^{2+}$  ion. The mean Cu-O distance for the four equatorial water molecules falls within a well defined range in these different studies, but the mean Cu-O distance for the axial water molecules has been more difficult to determine, due to interferences from the second-shell water molecules and, in some cases, from the counter-ions [35].

Five-fold coordination around the cupric ion with an average Cu-O distance of 1.96 Å was recently put forward in a combined neutron diffraction and CPMD effort [19]. The latest experimental studies, however, challenge the configuration with five equal bond lengths and suggest a distorted five- or distorted six-fold coordination [40, 41].

The CPMD simulation in Paper IV results in a first hydration shell consisting of five water molecules in a distorted square-pyramidal arrangement

around the  $\text{Cu}^{2+}$  ion with 4 equidistant equatorial water molecules, whose oxygen atoms lie approximately in a plane containing the ion, and with one axial water molecule at a longer distance from the ion. The second hydration shell contains 8 water molecules. Figure 3.2 shows an example of the hydration structure of the cupric ion, as obtained from the trajectory of the CPMD simulation.

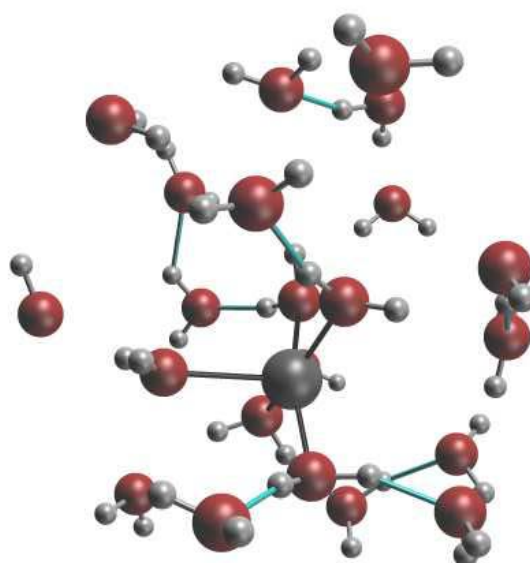
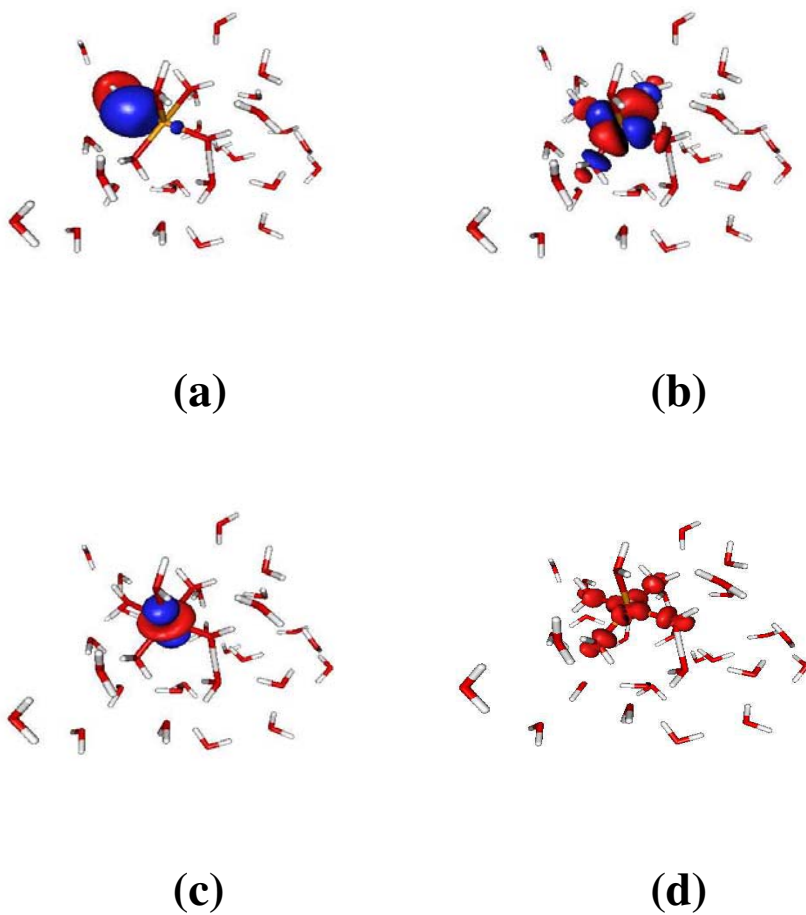


*Figure 3.2:* Snapshot of the water structure around an  $\text{Cu}^{2+}(aq)$  ion obtained from the CPMD trajectory. The water molecules surrounding the ion form an square pyramid.

Maximally Localized Wannier Functions (MLWFs) [42] and a spin density map have been calculated in order to illustrate the different bonding character between  $\text{Cu}^{2+}$  and the axial and equatorial water molecules. Figure 3.3a shows a bonding  $\sigma$  orbital formed between the  $\text{Cu}^{2+}$   $d_{x^2-y^2}$  orbital and a 2p lone-pair orbital on an equatorial water molecule (similar pictures exist for the other three equatorial water molecules). The MLWF in Figure 3.3b corresponds to

*Figure 3.3:* Snapshot taken from the CPMD simulation in Paper IV. (a) MLWF suggesting a mixing between the  $3d_{x^2-y^2}$  orbital of  $\text{Cu}^{2+}$  and the 2p lone-pair orbital of the O atom of one of the equatorial water molecules, forming a  $\sigma$  bonding orbital. (b) MLWF suggesting a strong mixing between the  $3d_{x^2-y^2}$  orbital of  $\text{Cu}^{2+}$  and the 2p lone-pair orbitals of the O atoms of the equatorial water molecules, forming a  $\sigma^*$  anti-bonding orbital. (c) MLWF corresponding to an unmixed  $3d_{z^2}$  orbital on  $\text{Cu}^{2+}$ . (d) Spin-density map.



the anti-bonding  $\sigma^*$  orbital, formed between the  $\text{Cu}^{2+}$   $d_{x^2-y^2}$  orbital and the four equatorial O 2p lone-pair orbitals. This is where the unpaired electron

is located, as can be seen on the spin density map in Figure 3.3d. Finally, the MLWF in Figure 3.3c essentially depicts an unmixed  $d_{z^2}$  orbital on  $\text{Cu}^{2+}$ . No strong participation from the axial water molecule is found. The  $\text{Cu}^{2+}$  ion is thus seen to participate in covalent bonding with the equatorial water molecules, while the axial water molecule appears to be only electrostatically bonded.

The main results of this section are the following:

- For the first hydration shell around the cupric ion five-fold coordination with 4 equidistant equatorial water molecules and one axial water molecule at a longer distance was found.
- Using MLWFs as a tool we find that the  $\text{Cu}^{2+}$  ion participates in covalent bonding with the equatorial water molecules, while the axial water molecule appears to be only electrostatically bonded.

### 3.3 Distance between the first and second hydration shells

The  $\text{O}\cdots\text{O}$  distances, calculated from the RDF between the water molecules in the first and second hydration shells for the different simulations are listed in Table 3.3 together with the corresponding experimental values. The experimental values are from X-ray diffraction experiments and IR measurements. Figure 3.4 illustrates the distance between first and second shell. For the sake of clarity most water molecules have been removed from the picture.

The absolute values for the  $\text{O}\cdots\text{O}$  distances are so strongly varying between different experiments and over time (i.e. years) [43] that a reliable comparison of the simulation results with experiment should focus on distance *differences* only. The shortening of the  $\text{O}\cdots\text{O}$  distance, due to the presence of a polyvalent ion, is substantial. The CPMD simulations reproduce the experimental shortening well and better than the classical MD simulations (except for simulations with polarizable models), since the many-body ion-hydration shell interactions are taken into account for all water molecules. Judging from the charge/Shannon's effective radii ratio, the shortening of the  $\text{O}\cdots\text{O}$  distance should be the largest for  $\text{Al}^{3+}$ . The fact that the CPMD simulation gives a smaller  $\text{O}\cdots\text{O}$  distance shortening for  $\text{Al}^{3+}$  might be a result of the small system size, due to which the water molecules in the second shell are influenced by the periodic images of the  $\text{Al}^{3+}$  ion.

The main results of the section are the following:

- We find  $\text{O}\cdots\text{O}$  shortenings from the CPMD simulations in agreement with experimental values.

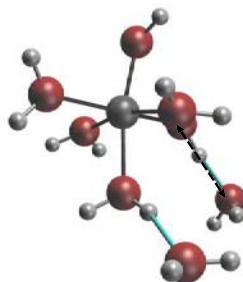


Figure 3.4: Illustration of the distance between the first and the second hydration shells.

Table 3.3: O···O distance between the first and the second hydration shells, calculated from the radial distribution functions from the CPMD and the CLMD simulations. Experimental literature values are taken from diffraction [35] and IR spectroscopy 36–38. Shortening of the O···O distance compared to pure liquid water is given in parenthesis. All distances are in Å.

| Method/ion | Fe <sup>2+</sup> | Fe <sup>3+</sup> | Cu <sup>2+</sup> | Al <sup>3+</sup> |
|------------|------------------|------------------|------------------|------------------|
| CPMD-32    | –                | 2.67 (0.15)      | 2.70 (0.12)      | 2.72 (0.10)      |
| CLMD-32    | –                | 2.64 (0.10)      | –                | –                |
| CLMD-512   | 2.69 (0.05)      | 2.64 (0.10)      | –                | –                |
| Experiment | (0.10)           | (0.07-0.18)      | (0.07-0.12)      | (0.07-0.18)      |

- For this property the CPMD simulations perform considerably better than the classical MD simulations based on effective pair potentials (many-body!).

### 3.4 Angular distribution of the water molecules around the metal ions

The orientations of first-shell and second-shell water molecules around  $\text{Fe}^{3+}$  (Paper **III**),  $\text{Cu}^{2+}$  (Paper **IV**) and  $\text{Al}^{3+}$  (Paper **V**) have been calculated in terms of the distribution of the tilt angle as a function of the distance from the ion and are shown as contour-maps in Figure 3.5. The tilt angle is here defined as a dihedral angle  $\theta_{\text{dihed}}$  [39]; see Figure 4 in Paper **III** and the text defining it. The average tilt angles in the first and second shells from the CPMD simulations are collected in Table 3.4 as  $180^\circ - \theta_{\text{dihed}}$ , in order to make the comparison with the literature results easier. We compare the results from the two classical MD simulations (32 water molecules and 512 water molecules) with the CPMD simulation of  $\text{Fe}^{3+}(\text{aq})$  (Paper **III**) and compare the orientations for  $\text{Fe}^{3+}$ ,  $\text{Cu}^{2+}$  and  $\text{Al}^{3+}$ .

For the first hydration shell around  $\text{Fe}^{3+}$ , the maxima for the angle  $\theta_{\text{dihed}}$  falls at  $\sim 180^\circ$ , i.e. the ion and the three water atoms lie in the same plane. The two classical simulations of  $\text{Fe}^{3+}(\text{aq})$  exhibit essentially the same distribution of the  $\theta_{\text{dihed}}$  angles close to  $180^\circ$  for the first shell, but the average angle differs by about  $10^\circ$  and the distribution is broader for the small box-size. The CPMD simulation yields a broader distribution compared to the classical simulations, which means a more flexible first hydration shell and more tilted water molecules. For the first hydration shell around  $\text{Al}^{3+}$ , we find a maximum for the angular distribution very close to the value for  $\text{Fe}^{3+}$ , while for the first hydration shell around  $\text{Cu}^{2+}$  the water molecules are much more tilted. The angular distribution is asymmetric for the copper case and the first shell is not clearly separated from the second, reflecting the very loose bonding of the axial water molecule.

*Table 3.4:* First and second shell water tilt angles, computed as  $180^\circ - \langle \theta_{\text{dihed}} \rangle$  from the three CPMD simulations. The experimental values (see Ref. [35]) are given in parenthesis.

|                             | $180^\circ - \theta_{\text{dihed}}$ (1 <sup>st</sup> shell) | $180^\circ - \theta_{\text{dihed}}$ (2 <sup>nd</sup> shell) |
|-----------------------------|---|---|
| $\text{Fe}^{3+}(\text{aq})$ | 23 (20;40)  | 55  |
| $\text{Cu}^{2+}(\text{aq})$ | 36 (42)   | –   |
| $\text{Al}^{3+}(\text{aq})$ | 24 (20;40)  | –   |

A comparison between CPMD and CLMD results can be made for  $\text{Fe}^{3+}$ , where the second-shell water molecules are found to be more tilted for the CPMD simulations, while the width of the distribution of the angles is similar to the classical simulations. No important size-dependence can be seen in the

contour-plots for the CLMD-32 and the CLMD-512 simulations. The angular-distribution plot for the second shell water molecules around  $\text{Al}^{3+}$  shows also a less common orientation for certain water molecules in the second hydration shell, possibly due to the fact that those water molecules are influenced by the periodic image of the metal ion. The region of the small angles (between 0 and  $90^\circ$ ) in Figure 3.5, where the hydrogen atoms of the water molecules point towards the ion has a non-negligible probability density for all three CPMD simulations.

The main results of the section are the following:

- The computed tilt angles for the water molecules in the first hydration shell agree quite well with the available experimental data.
- The first hydration shell is more flexible for the CPMD simulations compared to classical MD simulations.
- The angular distribution of the water molecules in the second shell is much broader for the simulations with 32 water molecules compared to the simulations with 512 water molecules. Also water molecules that are more tilted were observed for the smaller box, because these water molecules are more influenced by the periodic image of the metal ion.
- We find second-shell water molecules with their hydrogen atoms pointing towards the ion.

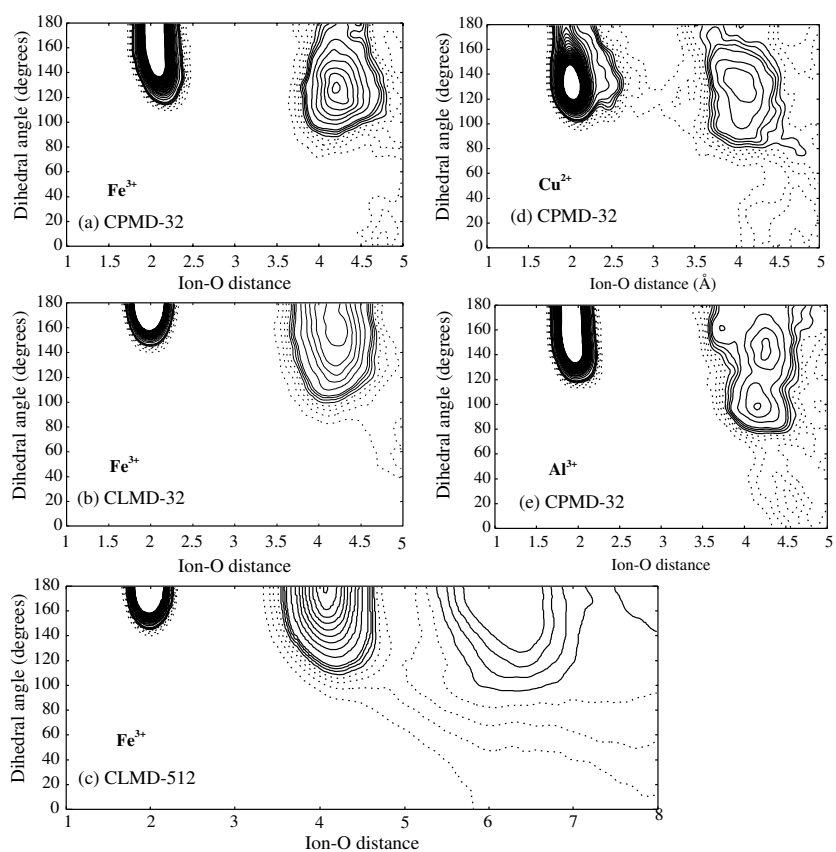


Figure 3.5: Angular-radial distribution functions for  $\text{Fe}^{3+}(aq)$ ,  $\text{Cu}^{2+}(aq)$  and  $\text{Al}^{3+}(aq)$ .

# Intramolecular vibrational properties of the water molecule

## 4.1 Experimental OH/OD frequencies

The presence of multivalent metal cations in aqueous solutions results in downshifts of the OD and OH vibrational frequency of the surrounding water molecules, as observed by infrared and Raman spectroscopic measurements. For liquid H<sub>2</sub>O, the experimental OH stretching frequency occurs at 3400 cm<sup>-1</sup> [44], downshifted by ca. 300 cm<sup>-1</sup> compared to the average value of the antisymmetric and the symmetric OD vibrations in the gas-phase H<sub>2</sub>O molecule (3707 cm<sup>-1</sup>). For liquid D<sub>2</sub>O, the experimental OD stretching frequency occurs at ~2500 cm<sup>-1</sup> [44], downshifted by ca. 220 cm<sup>-1</sup> compared to the average value of the antisymmetric and the symmetric OD vibrations in the gas-phase D<sub>2</sub>O molecule (2727 cm<sup>-1</sup>) [45].

For Fe<sup>3+</sup>(aq), no infrared spectroscopic data are available for the first-shell water molecules, but experimental results for other trivalent cations, such as Al<sup>3+</sup>, Cr<sup>3+</sup> and Rh<sup>3+</sup>, have been reported [38]. The experimental IR spectrum for water molecules in the first hydration sphere of Al<sup>3+</sup> shows an OD band centred around 2200 cm<sup>-1</sup>, i.e. downshifted by 525 cm<sup>-1</sup> with respect to the average gas-phase frequency; the corresponding OH band lies at ~2850 cm<sup>-1</sup>, i.e. downshifted by 860 cm<sup>-1</sup> with respect to the average gas-phase frequency. The experimental IR spectrum for the water molecules in the first hydration sphere around the cupric ion [37] shows a distortion of the hydration sphere due to the Jahn-Teller effect. An intense band lies at 2400 cm<sup>-1</sup>, corresponding to the more strongly bound equatorial water molecules and a weaker band at 2530 cm<sup>-1</sup>, caused by the axial water molecules. All experimental OH and OD frequencies normally correspond to *anharmonic* frequencies.

## 4.2 How to compute vibrational frequencies

Four types of intramolecular OH/OD vibrational frequencies have been computed in this thesis: (1) “classical VAC-FT” spectra; (2) “quantum-mechanical” anharmonic frozen-field spectra; (3) harmonic frozen-field spectra; (4) Harmonic normal-coordinate analysis from *ab initio* calculations. The first three frequencies are computed from MD simulations, the last one from

a geometry optimisation and a subsequent normal-mode coordinate analysis. A water model with intramolecular degrees of freedom, “SPC+CCL” was constructed in Paper I in order to study the vibrations of the water molecules in different MD simulations. The potential function is based on the simple point charge model (SPC) [46] combined with an accurate experimental intramolecular potential (CCL) [47].

#### 4.2.1 The “classical VAC-FT” spectra

The “classical” spectra were calculated by taking the Fourier transform of the Velocity Autocorrelation Function (VAC) for the relative velocities of the H/D atoms with respect to the velocity of the O atom, according to

$$f(\omega) \propto \int_0^{\infty} C_{vv}(t) \cos(\omega t) dt \quad (4.1)$$

where  $C_{vv}(t)$  is the velocity autocorrelation function, given by

$$C_{vv}(t) = \frac{1}{NM} \sum_i^N \sum_j^M (\vec{v}_i(t_j) \cdot \vec{v}_i(t_j + t)) \quad (4.2)$$

where the  $i$ -sum runs over the  $N$  contributing particles and the  $j$ -sum runs over all time origins  $t_j$ .

#### 4.2.2 The “quantum-mechanical” anharmonic frozen-field spectra

The anharmonic quantum-mechanical frozen-field vibrational spectra of the water molecules was constructed using the snapshots generated by the MD simulation. Here, the stretching vibrational frequencies of each water molecule were calculated from its interactions with the distorted, and “frozen”, water molecules surrounding the “central” molecule. For each snapshot and every selected water molecule, one OH bond was thus stretched and contracted in its “frozen” surroundings taken from the MD simulation and the sum of the inter- and intramolecular energies for each water molecule was calculated.

Each resulting OH potential energy curve was Taylor-expanded as:

$$V(r_{OH}) = V_0 + \frac{1}{2}k_2\Delta r_{OH}^2 + k_3\Delta r_{OH}^3 + \dots \quad (4.3)$$

where  $\Delta r_{OH} = r_{OH} - r_{e,OH}$ .

The variational solutions of the Schrödinger equation for the motion of the O-H oscillator in this anharmonic potential were then obtained by expanding the eigenfunctions into linear combinations of harmonic oscillator functions and solving the corresponding matrix equations. The anharmonic frequency was obtained from  $h\nu = E_0 - E_1$ .

### 4.2.3 The harmonic frozen-field spectra

For each oscillator *the harmonic frozen-field frequency* was calculated from the  $k_2$  term in the Taylor expansion above. The configurational broadening due to the different frozen-field environments produce the OH density-of-states spectrum, just as in the case of the anharmonic frequencies.

### 4.2.4 Harmonic normal-coordinate analysis from *ab initio* calculations

Harmonic vibrational frequencies were calculated for the fully optimised geometries of a water molecule and small  $\text{Al}(\text{D}_2\text{O})_n^{3+}$  clusters from *ab initio* calculations. The potential energy surface from the electronic structure calculation determines the vibrational frequencies. The vibrational frequencies are calculated from the second derivatives via a normal coordinate analysis and this general scheme is implemented in various quantum-mechanical programs. The harmonic frequencies in the Gaussian program are obtained from the diagonalisation of the force-constant matrix, in the CPMD program by finite differences of the first derivatives.

## 4.3 Vibrational frequencies: results from the simulations

### 4.3.1 Vibrations of the water molecule in the gas-phase

The calculation of the most simple model-system, the isolated water molecule, was a key test to evaluate the performance of the different methods used in this thesis. The calculated vibrational frequencies of  $\text{H}_2\text{O}(g)$  and  $\text{D}_2\text{O}(g)$  using different methods described above are presented in Table 4.1. The SPC+CCL model generates both *harmonic* and *anharmonic* frequencies that are very close to experiment. The “classical” VACF-FT frequency lies very close to the harmonic value, because the anharmonic part of the OH stretching potential is insufficiently sampled in the MD simulations [48]. The harmonic frequency from the CPMD calculation lies  $\sim 130 \text{ cm}^{-1}$  below the experimental value; the origin of this discrepancy will be addressed in section 4.4.

### 4.3.2 Vibrations of the water molecule in the pure liquid

The vibrational spectrum from the water molecules in the pure liquid has been computed from classical MD simulations with the SPC+CCL potential and from CPMD simulations. The calculated vibrational frequencies of the  $\text{H}_2\text{O}(l)$  and  $\text{D}_2\text{O}(l)$  and the gas-to-liquid shift are presented in Table 4.1. The

Table 4.1: OH/OD stretching frequencies for normal and deuterated water molecules in the gas-phase and in the liquid-phase from classical MD simulations with the SPC+CCL model and from CPMD simulations.

|                     |      | FT of VAC |                | Frozen-field spectra |                |       |             | Experimental |             |
|---------------------|------|-----------|----------------|----------------------|----------------|-------|-------------|--------------|-------------|
|                     |      | $\omega$  | $\Delta\omega$ | $\omega$             | $\Delta\omega$ | $\nu$ | $\Delta\nu$ | $\nu$        | $\Delta\nu$ |
| H <sub>2</sub> O(g) | CLMD | 3890      |                | 3890                 |                | 3720  |             | 3707         |             |
| H <sub>2</sub> O(l) | CLMD | 3590      | -300           | 3610                 | -280           | 3420  | -300        | 3400         | -310        |
| D <sub>2</sub> O(g) | CLMD | 2825      |                |                      |                |       |             | 2727         |             |
| D <sub>2</sub> O(g) | CPMD | 2695      |                |                      |                |       |             | 2727         |             |
| D <sub>2</sub> O(l) | CLMD | 2590      | -235           |                      |                |       |             | 2503         | -225        |
| D <sub>2</sub> O(l) | CPMD | 2340      | -355           |                      |                |       |             | 2503         | -225        |

SPC+CCL reproduces experimental liquid-phase frequencies and the gas-to-liquid shifts well, both for H<sub>2</sub>O(l) and D<sub>2</sub>O(l), as shown in Papers I and II. The results from the CPMD simulation are less convincing: the gas-to-liquid shift is too large by some 130 cm<sup>-1</sup>.

### 4.3.3 Vibrations of the water molecule in the solution

The vibrational spectrum from the water molecules in the first hydration shell around the polyvalent metal ions in this thesis has been computed from classical MD simulations with the SPC+CCL potential (Fe<sup>2+</sup>, Fe<sup>3+</sup>) and from CPMD simulations (Fe<sup>3+</sup>, Al<sup>3+</sup> and Cu<sup>2+</sup>). Figure 4.1 shows the classical, anharmonic and harmonic calculated OH stretching spectra for H<sub>2</sub>O(l) and the first-shell water molecules around Fe<sup>2+</sup> and Fe<sup>3+</sup> using the SPC+CCL water model.

We compare first the classical with the CPMD simulation of Fe<sup>3+(aq)</sup>. The simulated spectrum for the first-shell water molecules around Fe<sup>3+</sup> is downshifted by as much as  $\sim 500$  cm<sup>-1</sup> for both simulations with respect to the gas-phase frequency, and about half this value with respect to the pure liquid water frequency. The classical simulation with the set of potentials selected here performs well for the Fe<sup>3+(aq)</sup> solution. The not-so-perfect description of the OD stretching vibration by the CPMD method used here will be discussed in section 4.4.

The OD stretching frequencies from the CPMD simulations for the first-shell hydration water molecules around the trivalent ions Fe<sup>3+</sup> and Al<sup>3+</sup> are

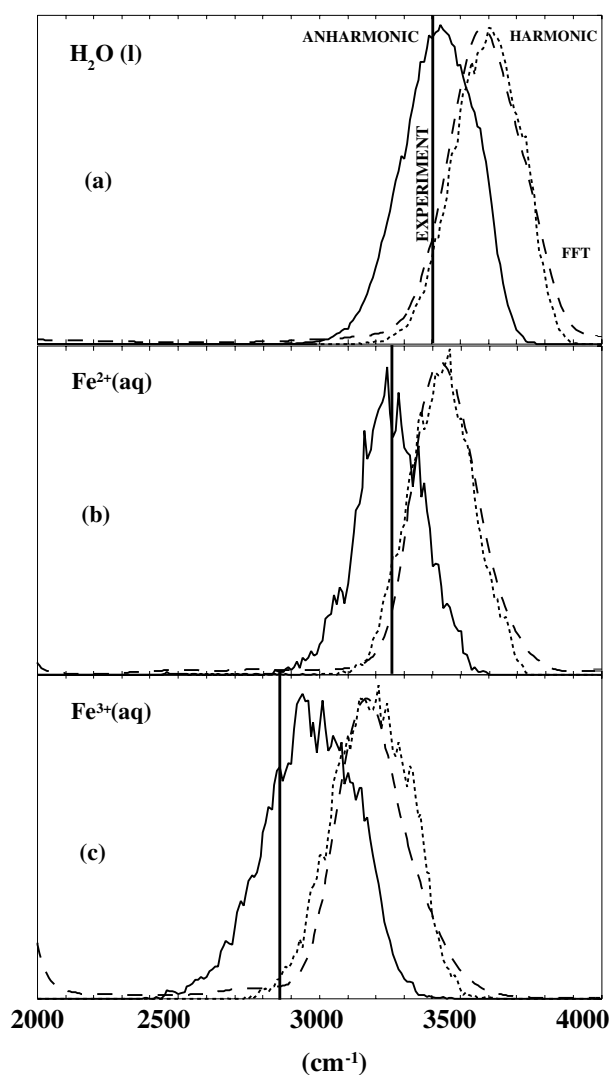


*Figure 4.1:* The classical, anharmonic and harmonic calculated OH stretching spectra for  $\text{H}_2\text{O}(l)$  and the first-shell water molecules around  $\text{Fe}^{2+}$  and  $\text{Fe}^{3+}$ . The experimental line for  $\text{Fe}^{3+}(aq)$  actually refers to  $\text{Al}^{3+}(aq)$ , since no experimental data for  $\text{Fe}^{3+}(aq)$  exists.

very close. The water molecules around  $\text{Cu}^{2+}$  have been divided in two groups: the four equatorial water molecules in a plane with the ion and the axial water molecule  $\sim 2.45 \text{ \AA}$  above that plane. For the equatorial water molecules, the downshift is  $\sim 120 \text{ cm}^{-1}$  with respect to liquid water and for the axial water molecule the simulated value falls slightly above the pure liquid value, both

Table 4.2: OD stretching frequencies (in  $\text{cm}^{-1}$ ) calculated for  $\text{D}_2\text{O}(g)$ ,  $\text{D}_2\text{O}(l)$  and the water molecules in the first hydration shells of  $\text{Cu}^{3+}$ ,  $\text{Fe}^{3+}$  and  $\text{Al}^{3+}$  from the CPMD simulations. The frequency shifts are given with respect to the isolated gas-phase molecule.

|   | CPMD-32  |                | CLMD     |                | Experiment |             |
|---|----------|----------------|----------|----------------|------------|-------------|
|   | $\omega$ | $\Delta\omega$ | $\omega$ | $\Delta\omega$ | $\nu$      | $\Delta\nu$ |
| $\text{D}_2\text{O}(g)$                           | 2695     |                | 2825     |                | 2727 [45]  |             |
| $\text{D}_2\text{O}(l)$                           | 2340     | -355           | 2590     | -235           | 2503 [44]  | -225        |
| $\text{Cu}^{2+}(aq)$ , 1 <sup>st</sup> shell (ax) | 2390     | -305           |          |                | 2530 [37]  | -200        |
| $\text{Cu}^{2+}(aq)$ , 1 <sup>st</sup> shell (eq) | 2215     | -480           |          |                | 2400 [37]  | -325        |
| $\text{Fe}^{3+}(aq)$ , 1 <sup>st</sup> shell      | 2160     | -535           | 2330     | -500           | 2200 [38]  | -525        |
| $\text{Al}^{3+}(aq)$ , 1 <sup>st</sup> shell      | 2130     | -525           |          |                | 2200 [38]  | -525        |

results in agreement with experiment. The CPMD simulations gives a qualitatively sound description of the OD stretching frequencies. The discrepancy between the experimental data and the absolute frequencies and the frequency shifts calculated from the CPMD simulations is addressed in the next section.

## 4.4 Vibrational frequencies from CPMD simulations versus experiment

The most important factors that can be responsible for the discrepancy between the calculated and the experimental frequencies in the CPMD simulations are the following: (i) the CPMD box-size; (ii) the fictitious electron mass parameter in CPMD simulations; (iii) the exchange-correlation functional; (iv) anharmonicity effects. In Paper V, the hydration of  $\text{Al}^{3+}$  was treated as a test case to investigate the origin of the discrepancy between the frequencies calculated from the CPMD simulations and the experimental frequencies. The purpose of that exercise was to shed some light on the magnitude and the signs of the errors involved in the comparison.

### 4.4.1 The CPMD box-size

In Paper III the OD frequency dependence on the box-size was studied for  $\text{Fe}^{3+}(aq)$  using classical force-field MD simulations. The frequencies for the first-shell water molecules were shifted by approximately  $+40 \text{ cm}^{-1}$  when the box-size increased from 32 to 512 water molecules. The small box-size was

thus found to lower the calculated absolute frequencies, but not by much, and only for the ionic aqueous solution.

#### 4.4.2 The fictitious electron mass parameter in CPMD simulations

Previous studies [49, 50] have demonstrated the necessity to also check the dependence of the results of CPMD simulations on the value of the fictitious electron mass parameter ( $\mu$ ) because, for common values of this parameter, a systematic bias may affect the Car-Parrinello forces, due to the drag from the fictitious electron mass. The dependence of the OD frequencies on the drag from the fictitious electron mass was checked by performing several short CPMD simulations of a single  $\text{D}_2\text{O}(g)$  molecule using three different values of the  $\mu$  parameter. The OD stretching frequencies, for the different values of  $\mu$  ( $\mu=900, 400$  and  $200$  a.u.) were found to be strongly affected by the choice of the fictitious electron mass. For  $\mu=900$  a.u. in particular, which is the value used in the CPMD runs in this thesis, the average OD stretching frequencies deviate  $\sim 250 \text{ cm}^{-1}$  from the ideal harmonic values.

The frequencies can be corrected the drag from the fictitious electron mass (see ref. 49), according to a rigid ion model, using

$$\omega_{\text{corrected}} = \omega_{\text{CP}} \sqrt{1 + \Delta M/M}, \quad (4.4)$$

where  $\omega_{\text{CP}}$  is the frequency extracted directly from the CPMD simulation and  $\Delta M/M$  the mass-correction term. For  $\mu=900$  a.u., the scaling factor for the frequencies is 1.082.

If the gas-phase correction value is assumed to be valid also for the liquid phases, the fictitious mass correction leads to substantial upshifts of the calculated OD frequencies (by **+200  $\text{cm}^{-1}$**  for liquid water and by **+180  $\text{cm}^{-1}$**  for the first-shell water molecules around  $\text{Al}^{3+}$ ).

#### 4.4.3 The BLYP functional

The high-level *ab initio* frequency calculations for the water monomer and for the  $\text{Al}(\text{D}_2\text{O})_n^{3+}$  clusters in Paper V showed that the BLYP functional produces an absolute value of the harmonic vibrational frequency for the monomer lower by approximately **+100  $\text{cm}^{-1}$** .

#### 4.4.4 Anharmonicity effects

The intramolecular stretching vibrations in the water molecule are very anharmonic, and the OD stretching band for a bound water molecule bound is generally downshifted a lot due to anharmonicity, and the stronger the intermolecular bonding, the larger the anharmonicity shift (see, for example,

Berglund et al. [51]). A comparison of the calculated essentially harmonic CPMD-frequencies with the experimental anharmonic ones, needs to take this effect into account. This anharmonicity error in the OD frequencies for water in the first hydration shell is around **-100 cm<sup>-1</sup>**. Intensity weighting of the spectra will shift the frequencies another **-30** for pure liquid water [52] and **-50 cm<sup>-1</sup>** for the solution [53].

The main conclusions from this chapter are the following:

- Our flexible water model, SPC+CCL, constructed from the intermolecular SPC water-water potential and the experimental gas-phase intramolecular CCL potential, produces correct anharmonic and harmonic frequencies for the O-H and O-D stretch both in the gas-phase and in the liquid phase. The SPC+CCL model combined with the Curtiss Fe<sup>n+</sup>-water model gives frequency shifts for water molecules in the first hydration shell of the ferric and ferrous ion that are close to experiment.
- Shortcomings in the BLYP functional used in the CPMD simulations shift the absolute values of the OD frequency downwards by more than 100 cm<sup>-1</sup>.
- The drag of the electrons due to the fictitious electron mass in the CPMD simulations shifts the OD stretching frequencies downwards by several hundred cm<sup>-1</sup> for commonly used electron masses.
- The box-size of 32 water molecules introduces a relatively small error (upwards) for the OD frequencies in the first ionic shell.
- The lack of taking anharmonicity into account in the CPMD simulations shift the absolute OD frequencies upwards by some hundred cm<sup>-1</sup>.

## Summary and concluding remarks

The main results of this thesis work are:

- Good overall agreement between CPMD simulations and experiment for the structural properties of the hydration shells.
- Certain properties seem to be differently and certain other properties seem to be better described by CPMD than by CLMD (using the empirical potentials from the literature).
  - The CPMD simulations describe the O···O shortening better than the CLMD simulations.
  - The CPMD simulations yield a rather broad distribution of water tilt angles in the first shell, compared to CLMD for the ferric ion.
  - For the CPMD simulations there are second-shell water molecules with their hydrogen atoms pointing towards the ion, but not for the CLMD simulations.
- CPMD enables the study of a transition metal complex where the covalent ion-ligand bonding and the electronic structure of the ion play a role in determining the coordination figure.
- To pinpoint the consequences of using a small system-size a CLMD simulation with 1 Fe<sup>3+</sup> ion and 512 water molecules was compared with an identical simulation, using only 1 Fe<sup>3+</sup> ion and 32 water molecules (as in the CPMD simulations). The small system size affects the orientation of the water molecules in the second hydration shell and the O-D stretching frequency of the first shell water molecules around the ferric ion.
- An analytical potential, constructed as a sum of a “perfect” (experimental) intramolecular potential (CCL) and an established effective pair potential (SPC for liquid water and the Curtiss potentials for Fe<sup>n+</sup>-water) manages to reproduce experimental frequencies and frequency shifts very well (as well as hydration structure, ionic diffusion and residence times).

- To make a comparison of the CPMD-derived frequencies with experimental frequencies possible, the influence of a number of systematic effects have been addressed, such as the exchange-correlation functional, the fictitious electron mass, anharmonicity effects and the small box-size in the simulation. Each of these factors (except the last one) are found to affect the OD frequency by a hundred  $\text{cm}^{-1}$  or more.

There are different ways to further improve the CPMD simulations of metal ions in aqueous solution presented in this thesis work. The exchange-correlation functionals used in this thesis are far from perfect. One important way to refine the electronic structure calculations is to improve the quality of the available exchange-correlation functionals and major efforts are being made to achieve this goal. This work (among others) has shown one of the consequences of having a high fictitious electron mass in the CPMD simulations. A lower fictitious electron mass is therefore preferable, although it comes at the cost of lowering the timestep, making the CPMD simulations even more computationally expensive. The development of faster computers will allow for CPMD simulations with a larger number of solvent molecules, longer simulations and a larger number of simulations.

## Acknowledgments

I would like to thank my supervisor Kersti Hermansson for her support and for sharing her knowledge. Special thanks to Daniel Spångberg who introduced me to the more practical aspects of this field and gave useful advice and help all the way through these four years.

I would also like to thank my friends and colleagues at Materials Chemistry (past and present) and especially the members of the theoretical group: Anders, Björn, Carsten, Christopher, David, Greg, Micke, Pavlin, Somkiat, Tore and Vladimir.

Ulrika Bergvall, Eva Larsson and Gunilla Lindh are thanked for their excellent administrative support and Peter Lundström, NOE and Anders Lund for computer-related trouble-shooting.

I have found interesting company and good friends at other departments in The Ångström Laboratory, at SLU (great summertime BBQs!) and in the wider world outside the university.

Financial support from the European FP5 IHP program (Research Training Network Contract No. HPRN-CT-2000-19) is hereby acknowledged.

Finally, I would like to thank my relatives for their support and encouragement during all these years.



## References

- [1] D.T. Richens, *The Chemistry of Aqua Ions*, Wiley, Chichester, 1997.
- [2] S.W. Rick and S.J. Stuart Potentials and algorithms for incorporating polarizability in computer simulations. In *Reviews in Computational Chemistry, Vol. 18*, K.B. Lipkowitz and D.B. Boyd, Eds. Wiley, New York, 2002.
- [3] T. Kerdcharoen, K.R. Liedl and B.M. Rode, *Chem. Phys.* **211**, 313 (1996).
- [4] A. Tongraar, K.R. Liedl and B.M. Rode, *Chem. Phys. Lett.* **268**, 56 (1998).
- [5] H.H. Loeffler and B.M. Rode, *J. Chem. Phys.* **117**, 110 (2002).
- [6] R. Armunanto, C.F. Schwenk and B. M. Rode, *J. Phys. Chem. A* **107**, 3132 (2003).
- [7] R. Car and M. Parrinello, *Phys. Rev. Lett.* **55**, 2471 (1985).
- [8] R. Parr and W. Yang, *Density Functional Theory of Atoms and Molecules*, Oxford University Press, New York, 1989.
- [9] A.P. Lyubartsev, K. Laasonen and A. Laaksonen, *J. Chem. Phys.* **114**, 3120 (2001).
- [10] D. Marx, M. Sprik and M. Parrinello, *Chem. Phys. Lett.* **273**, 360 (1997).
- [11] J.A. White, E. Schwegler, G. Galli and F. Gygi, *J. Chem. Phys.* **113**, 4668 (2000).
- [12] R. Vuilleumier and M. Sprik, *J. Chem. Phys.* **115**, 3454 (2001).
- [13] F.C. Lightstone, E. Schwegler, R.Q. Hood, F. Gygi and G. Galli, *Chem. Phys. Lett.* **343**, 549 (2001).
- [14] T. Ikeda, M. Hirata and T. Kimura, *J. Chem. Phys.* **119**, 12386 (2003).
- [15] L. Ramaniah, M. Bernasconi and M. Parrinello, *J. Chem. Phys.* **109**, 6839 (1998).
- [16] I. Bakó, J. Hutter and G. Pálincás, *J. Chem. Phys.* **117**, 9838 (2002).
- [17] M. Naor, K. Van Nostrand, and C. Dellago, *Chemical Physics Letters* **369**, 159 (2003).
- [18] B. Ensing and E.J. Baerends, *J. Phys. Chem. A* **106**, 7902 (2002).
- [19] A. Pasquarello, I. Petri, P.S. Salmon, O. Parisel, R. Car, E. Tóth, D.H. Powell, H.E. Fischer, L. Helm and A.E. Merbach, *Science* **291**, 856 (2001).
- [20] J. Blumberger, L. Bernasconi, I. Tavernelli, R. Vuilleumier and M. Sprik, *J. Am. Chem. Soc.* **126**, 3928 (2004)
- [21] R.G. Pearson, *J. Chem. Educ.* **45**, 643 (1968).
- [22] R.G. Pearson, *Inorg. Chem.* **27**, 743 (1988).
- [23] R.D. Shannon, *Acta. Cryst. A* **32**, 751 (1976).

- [24] J.K. Beatti, S.P. Best, B.W. Skelton and A.H.J White, *J. Chem. Soc., Dalton Trans.* 2105 (1981).
- [25] W.C. Swope, H.C. Andersen, P.H. Berens and K.R. Wilson, *J. Chem. Phys.* **76**, 637 (1982).
- [26] L.A. Curtiss, J.W. Halley, J. Hautman and A. Rahman, *J. Chem. Phys.* **86**, 2319 (1987).
- [27] S. Nosé, *Mol. Phys.* **52**, 255 (1984).
- [28] W.G. Hoover, *Phys. Rev.* **A31**, 1695 (1985).
- [29] M.P. Allen and D.J. Tildesley, *Computer Simulations of Liquids*, Clarendon Press, Oxford, 1987.
- [30] A. Szabo and N.S. Ostlund, *Modern Quantum Chemistry*, McGraw-Hill, New York, 1989.
- [31] D. Marx and J. Hutter, *Modern Methods and Algorithms of Quantum Chemistry*, Forschungszentrum Jlich, NIC Series, Vol. 1, 2000.
- [32] D. Vanderbilt, *Phys. Rev. B* **41**, 7892 (1990).
- [33] J. Burgess, *Metal Ions in Solution*, Ellis Horwood, Chichester, 1978.
- [34] Bolhuis, P. G., D. Chandler, C. Dellago, and P. Geissler, *Ann. Rev. of Phys. Chem.* **59**, 291 (2002).
- [35] H. Ohtaki and T. Radnai, *Chem. Rev.* **93**, 1157 (1993).
- [36] O. Kristiansson, A. Eriksson and J. Lindgren, *Acta. Chem. Scand.* **A38**, 613 (1984).
- [37] B. Beagley, A. Eriksson, J. Lindgren, I. Persson, L.G.M. Pettersson, M. Sandström, U. Wahlgren and E.W. White, *J. Phys.: Condens. Matter* **1**, 2395 (1989).
- [38] P.-Å. Bergström, J. Lindgren, M. Read and M. Sandström, *J. Phys. Chem.* **95**, 7650 (1991).
- [39] D. Spångberg and K. Hermansson, *J. Chem. Phys.* **120**, 4829 (2004).
- [40] M. Benfatto, P. D'Angelo, S. Della Longa and N.V. Pavel, *Phys. Rev. B* **65**, (2002).
- [41] I. Persson, P. Persson, M. Sandström and A.-S. Ullström, *J. Chem. Soc. Dalton Trans.* 1256 (2002).
- [42] N. Marzari and D. Vanderbilt, *Phys. Rev. B* **56**, 12847 (1997).
- [43] J.M. Sorenson and G. Hura and R.M. Glaeser and T. Head-Gordon, *J. Chem. Phys.*, **113**, 9149 (2000).
- [44] H.R. Wyss and M. Falk, *Can. J. Chem.* **48**, 607 (1970).
- [45] W.S. Benedict and N. Gailar and E.K. Plyler, *J. Chem. Phys.* **24**, 1139 (1956).
- [46] H.J.C. Berendsen, J.P.M. Postma, E.F. van Gunsteren and J. Hermans, in: B. Pullman, ed., *Intermolecular forces*, D. Reidel, Dordrecht, 1981.
- [47] G.D. Carney and L.A. Curtiss and S.R. Langhoff, *J. Mol. Spectrosc.* **61**, 371 (1976).
- [48] L. Ojamäe and K. Hermansson, *Chem. Phys. Lett.* **191**, 500 (1992).
- [49] P. Tangney and S. Scandolo, *J. Chem. Phys.* **116**, 14 (2002).
- [50] B. Kirchner and J. Hutter, *J. Chem. Phys.* **121**, 5133 (2004).

- [51] B. Berglund, J. Lindgren and J. Tegenfeldt, *J. Mol. Struct.* **43**, 169 (1978).  
[52] K. Hermansson, S. Knuts and J. Lindgren, *J. Chem. Phys.* **45**, 7486 (1991).  
[53] L. Pejov and K. Hermansson, *J. Mol. Liq.* **98-99**, 367 (2002).

# Acta Universitatis Upsaliensis

*Digital Comprehensive Summaries of Uppsala Dissertations  
from the Faculty of Science and Technology 38*

Editor: The Dean of the Faculty of Science and Technology

A doctoral dissertation from the Faculty of Science and Technology, Uppsala University, is usually a summary of a number of papers. A few copies of the complete dissertation are kept at major Swedish research libraries, while the summary alone is distributed internationally through the series Digital Comprehensive Summaries of Uppsala Dissertations from the Faculty of Science and Technology. (Prior to January, 2005, the series was published under the title "Comprehensive Summaries of Uppsala Dissertations from the Faculty of Science and Technology".)

Distribution: [publications.uu.se](http://publications.uu.se)  
urn:nbn:se:uu:diva-5742



ACTA  
UNIVERSITATIS  
UPSALIENSIS  
UPPSALA  
2005